Scattering matrix elements of biological particles measured in a flow through system: theory and practice

Peter M. A. Sloot, Alfons G. Hoekstra, Hans van der Liet, and Carl G. Figdor

Light scattering techniques (including depolarization experiments) applied to biological cells provide a fast nondestructive probe that is very sensitive to small morphological differences. Until now quantitative measurement of these scatter phenomena were only described for particles in suspension. In this paper we discuss the symmetry conditions applicable to the scattering matrices of monodisperse biological cells in a flow cytometer and provide evidence that quantitative measurement of the elements of these scattering matrices is possible in flow through systems. Two fundamental extensions to the theoretical description of conventional scattering experiments are introduced: large cone integration of scattering signals and simultaneous implementation of the localization principle to account for scattering by a sharply focused laser beam. In addition, a specific calibration technique is proposed to account for depolarization effects of the highly specialized optics applied in flow through equipment.

I. Introduction

Simultaneous measurement of elastic light scattering (ELS) and fluorescence in a flow through system is an important tool in biological sciences to identify and separate various populations of blood cells. Especially the availability of numerous monoclonal antibodies, labeled with fluorescent probes, specific for subsets of human cells allow rapid identification and subsequent isolation in a flow cytometer (FCM).[1-3] This FCM technique exploits hydrofocusing of cell suspension by means of a sheath flow. The forced linear array of localized cells can be irradiated by a sharply focused laser beam. The cells can be identified and isolated with respect to the fluorescence signal specific for the various labeled subpopulations. In addition a light scattering signal, simultaneously measured with the fluorescence signal, is commonly used to trigger the data acquisition equipment.[3]

Staining of cells with fluorescent probes may affect the cell function and complicate cell preparation.[4] Therefore alternative pathways to characterize the cells, or cellular particulates, were recently investigated. It was already shown by Salzmann et al. that

simultaneous detection of forward scattering (FS) and side scattering (SS) allows identification of various populations of human peripheral blood cells.[5] Both experimental and theoretical studies were performed to unravel the complete angular ELS spectrum for living cells.[6-9] Various other light scattering experiments have been proposed since. It was suggested, for example, to measure differential light scattering from cells that were simultaneously irradiated by two laser beams tuned to different wavelengths.[10] Other experiments include angular ratio measurement and small angle detection techniques.[9,11] However, due to the short sampling time characteristic for FCM measurements (typical values are ~10 μs/cell), the scope of possible light scattering experiments is limited.[3]

In a previous paper we proposed a modified Rayleigh-Debye-Gans (mRDG) theory to approximate numerically the light scattering information present in nucleated blood cells such as human peripheral lymphocytes.[12-14] It was shown that the simultaneous measurement of FS, SS, and backscattering (BS) is well suited to characterize various physical properties of biological cells. Parts of these theoretical calculations were recently confirmed by experimental data.[14] Although, theories based on (m)RDG approximations allow rapid calculation of angular light scattering spectra from complex structures, no information on the (de)polarization introduced by the particle is available. It was shown by Bickel et al.[15] that the information content of the scattering matrix elements allows detailed differentiation of various subcellular particles. Especially, minute structural modifications of the scatterer are reflected by the scattering matrix

elements.[15,16] These types of experiment however cannot be readily implemented in a flow through system, since the light scattering signal of each cell (or cell suspension) must be measured over too large a period of time. As a consequence, the measurement of significant Mueller matrix elements in a FCM has not yet attained much attention. Despite these experimental complications, implementation of the (de)polarization of the scattered light into a FCM is very promising, since the scattering signals can be applied to discriminate and separate various populations of biological particles. Thus far only one qualitative experiment, concerning cross polarization of subsets of human granulocytes in flow, has been reported in the literature.[17]

In this study we provide evidence that the most significant Mueller matrix elements for nucleated blood cells can be obtained from light scattering experiments in a flow through system.

Section II describes the theoretical considerations related to the polarization status of light scattered by an ensemble of human blood cells measured in a flow through system. In Sec. III we describe experimental methods to investigate whether flow through equipment is suited for quantitative determination of the scattering matrices of particles in flow. To interpret the experimental data, we applied the generalized Lorenz Mie theory (GLMT) and simultaneously calculated the integrated light scattering intensities.[18] To facilitate rapid numerical calculations, a Mie scattering program[19] was modified by implementation of the localization principle.[20-22] In addition a newly developed calibration technique for special purpose optics is presented. In Sec. IV measurements and corresponding theoretical calculations of scattering matrix elements of monodisperse polystyrene particles in a flow through system are discussed.

In the discussion (Sec. V) we extrapolate the experimental results and the theoretical considerations to investigate the characteristics of the scattering matrix elements for nucleated blood cells. Finally the RDG regime, with respect to Mie theory, is discussed for particles resembling the low symmetry properties of human blood cells.

II. Theory

A. Scattering Matrix

In this section we describe the polarization states of light incoherently scattered by an ensemble of human blood cells measured in a flow through system. The scattering geometry is depicted in Fig. 1. A single particle flows in the positive x-direction and is illuminated by a sharply focused laser beam that propagates in the positive z-direction. The scattering direction $\hat{e}_s$ and the forward direction $\hat{e}_z$ define the scattering plane. Three detectors collect the scattered light in the forward scattering (FS), side scattering (SS), and backscattering (BS) directions. The differential angles $\Delta\theta$ and $\Delta\phi$ define the numerical aperture of each detector. The polarization properties of light, propagating through a linear medium (i.e., a cell), are com-
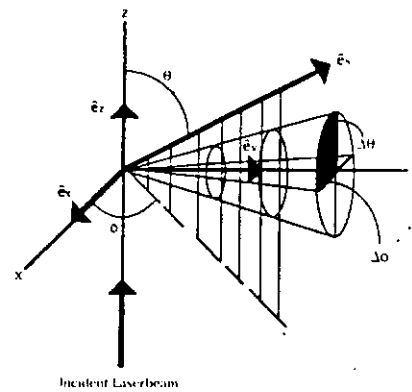

Fig. 1. Scattering geometry.

pletely described by the elements I, Q, U, V of the Stokes vector $\vec{S}$:

$$I = \langle E_l E_l^* + E_r E_r^* \rangle,$$
$$Q = \langle E_l E_l^* - E_r E_r^* \rangle,$$
$$U = \langle E_l E_r^* + E_r E_l^* \rangle,$$
$$V = i\langle E_l E_r^* - E_r E_l^* \rangle.$$

(1)

The subscripts l and r refer to the components of the scattered electric field parallel and perpendicular to the scattering plane, respectively. The brackets indicate time averages. The polarization state of the incident beam can be changed on interaction with a scatterer (i.e., a cell). The Stokes vectors of the incident beam and the scattered beam are related by a 4 × 4 matrix:

$$\begin{bmatrix} I \\ Q \\ U \\ V \end{bmatrix}_s = \frac{1}{k^2 R^2} \begin{bmatrix} S_{11} & S_{12} & S_{13} & S_{14} \\ S_{21} & S_{22} & S_{23} & S_{24} \\ S_{31} & S_{32} & S_{33} & S_{34} \\ S_{41} & S_{42} & S_{43} & S_{44} \end{bmatrix} \begin{bmatrix} I \\ Q \\ U \\ V \end{bmatrix}_i,$$

(2)

where the index i indicates the Stokes vector of the incident beam and s indicates the Stokes vector of the scattered beam, $k = 2\pi/\lambda$ (λ is the wavelength of the incident light), and R denotes the distance to the detector.[19,20] The scattering or Mueller matrix contains complete information of the incoherent elastic light scattering properties of a particulate system. In flow cytometers, a cell suspension is introduced into a hydrofocusing cuvette.[2] When the cells enter the cuvette, they are randomly oriented. Application of a sheath fluid results in a long file of cells that pass one by one the focus plane of the incident light. Although the hydrodynamic forces introduce some secondary orientation of the cells, the ensemble of cells passing the laser beam can still be considered as a collection of random oriented particles.[3,23-27] Ensemble averages are identical to time averages when symmetry conditions are concerned.[19] Therefore the symmetry properties of cell suspension can be deduced from the combined symmetry properties of cells from that particular suspension, studied one by one. In addition, sequential illumination of the cells guarantees that no systematic relation among the individual particles is present. This incoherent scattering allows one to sum all the scattering matrices of the individual
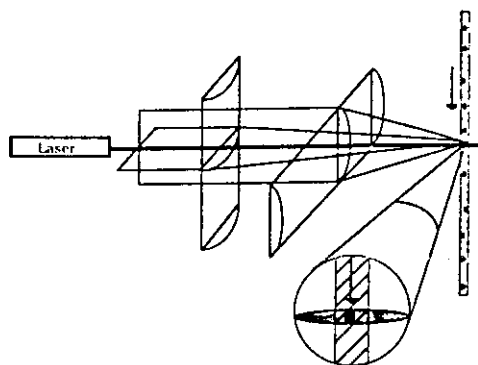
Fig. 2. Illumination of a linear array of particles by means of a sharply focused laser beam. The dark grey area indicates the focused laser beam. The particles are represented by black dots.

particles. As a consequence, the symmetry condition of the complete ensemble will reduce the number of independent elements in the scattering matrix.

Since in typical biological experiments homogeneous populations of $\sim 10^5$ cells are studied, it is assumed that each cell from a particular population has both mirror and reciprocal cells that pass the laser beam.[2-4] The matrix of Eq. (2) reduces in accordance with this assumption to[20]

$$\begin{bmatrix} S_{11} & S_{12} & 0 & 0 \\ S_{12} & S_{22} & 0 & 0 \\ 0 & 0 & S_{33} & S_{34} \\ 0 & 0 & -S_{34} & S_{44} \end{bmatrix}. \quad (3)$$

This scattering matrix essentially describes the scattering properties of an arbitrary monodisperse cell population measured in a flow system.

A test system of well-defined polystyrene spheres was selected to investigate the possibility of quantitative measurement of the independent Mueller matrix elements [Eq. (3)] in a FCM. The elements of the related scattering matrix $\bar{M}$ can be calculated exactly:

$$\bar{M} = \begin{bmatrix} S_{11} & S_{12} & 0 & 0 \\ S_{12} & S_{11} & 0 & 0 \\ 0 & 0 & S_{33} & S_{34} \\ 0 & 0 & -S_{34} & S_{33} \end{bmatrix}. \quad (4)$$

B. Illumination of Particles in a Flow Through System

Sequential one by one illumination of an array of particles passing a laser beam in a FCM requires extreme focusing of the laser field. In our apparatus, sharp focusing up to cellular dimensions (~ 3.5 by 16 μm for $\lambda = 632.8$ nm) was achieved by means of two crossed cylindrical lenses (focal lengths of 7.5 and 1.5 cm, see Fig. 2).[4]

The scattering of a particle in a sharply focused laser beam cannot be described by the conventional plane wave equations obtained by Mie. A solution to this problem is formulated by the general Lorenz Mie theory (GLMT) that has been recently discussed.[28,29] This theory is well suited to describe the scattering of a Gaussian beam by a spherical, isotropic, homogeneous, and nonmagnetic particle, with an arbitrary location

with respect to the beam axis. The GLMT incorporates the field components of a real laser beam, with a TEM_{00} Gaussian mode, in the amplitude coefficients of Mie functions. We propose therefore to calculate the elastic light scattering of spheres in a FCM by means of this GLMT. For a homogeneous sphere the scattering intensities I_θ and I_ϕ, associated with the fields E_θ and E_ϕ (Fig. 1), are defined by

$$I_\phi(\theta) = \frac{\lambda^2}{4\pi^2 R^2} |S_1(\theta)|^2 \quad \text{and} \quad I_\theta(\theta) = \frac{\lambda^2}{4\pi^2 R^2} |S_2(\theta)|^2,$$

with amplitude functions

$$S_1(\theta) = \sum_{n=1}^{\infty} \frac{2n+1}{n(n+1)} g_n[a_n \pi_n(\cos\theta) + b_n \tau_n(\cos\theta)],$$

$$\quad (5)$$

$$S_2(\theta) = \sum_{n=1}^{\infty} \frac{2n+1}{n(n+1)} g_n[a_n \tau_n(\cos\theta) + b_n \pi_n(\cos\theta)],$$

where g_n is a weighting function that describes the field expansion of the Gaussian beam in the GLMT. The Mie scattering coefficients a_n and b_n are obtained from the Ricatti-Bessel functions, whereas π_n and τ_n are derived from the associated Legendre polynomials $[P_n(\cos\theta)]$.[20]

Due to the complex structure of the formal solution for g_n, computational difficulties may arise.[28] Some simplifications can be obtained if the partial wave components of the incident field (a_n and b_n) are associated with localized incident geometrical rays.[20] This so-called localization principle (LP) associates the partial wave components of order n to a corresponding incident ray, passing the origin of the scatterer at a distance $(n + 1/2)\lambda/2\pi$. The LP gives a physical interpretation of the asymptotic behavior of the Ricatti-Bessel functions that appear in a_n and b_n when $n + 1/2 > \alpha$ (α is the size parameter of the particle: $\alpha = 2\pi r/\lambda$). The LP simplifies the computational algorithm for Mie scattering by a homogeneous sphere in an axisymmetric Gaussian beam enormously. The number of terms n that need to be calculated, for example, reduces to approximately $n \approx \alpha$.[20] In addition, it can be shown that g_n in Eq. (5) transforms to[21]

$$g_n = \exp\left\{-\left[\frac{(n+1/2)\lambda}{2\pi\omega_0}\right]^2\right\}, \quad (6)$$

where ω_0 is the beam waist radius of the axisymmetric Gaussian laser beam.

Both simplifications are implemented in the numerical calculations of the Mueller matrix elements to verify the experimental data.

C. Calculation of the FS, SS, and BS Intensities

In contrast to conventional scattering equipment, the detectors in a flow cytometer are located close to the scattering entity. As a consequence, relatively large numerical apertures are involved. Therefore, the calculated scattering intensities must be integrated over a large cone in the FS, SS, and BS directions. The total intensity measured by a detector surface element $R^2 \sin\theta d\theta d\phi$ is

$$I_{FS,BS} = \frac{I_0}{k^2 R^2} \int_\phi \int_\theta R^2 I(\theta) \sin(\theta) d\theta d\phi, \qquad (7a)$$

where $I(\theta)$ is the calculated intensity from the GLMT program.

As can be seen in Fig. 1, ϕ ranges from 0 to 2π for both the FS and the BS. A beam stop was inserted to remove the primary beam from the sensitive area of the FS detector, whereas in the BS direction a hole in the detector partially removed the backward scattered light. In the SS direction, however, $\Delta\phi = \Delta\theta$, and it follows that

$$I_{SS} \approx \int_{90-\Delta\theta}^{90+\Delta\theta} I(\theta) r(\theta,\phi) d\phi, \qquad (7b)$$

where $r(\theta,\phi) = 2.0\{(\Delta\phi)^2 - (90 - \theta)\}^{1/2}$. These intensities can be calculated for all the scattering matrix elements in Eq. (4).

III. Experimental Methods

In the previous section arguments were provided that correct measurement of the four independent matrix elements $(S_{11}, S_{12}, S_{33}, S_{34})$ is a necessity to demonstrate that the equipment is suited for quantitative measurement of the scattering matrices of biological cells.

The elements of Eq. (4) can be obtained by means of various combinations of polarizing filters in the incident beam (polarizer P) and in the scattered beam(s) (analyzer A).[30,31] For example, the elements S_{11} and S_{12} can be derived from subsequent measurement of $\{P_{\parallel},A_+\}$ and $\{P_{\perp},A_+\}$. The subscripts $\parallel, \perp, +, -$ refer to linear polarizers with optical axes parallel, perpendicular, $+45°$, and $-45°$ with respect to the scattering plane, respectively. Circular polarizers are denoted by P_R, P_L for right- and left-handed circular polarization. The combination $\{P_{\parallel},A_+\}$, for example, results in $\frac{1}{4}(S_{11} + S_{12})$. This can be demonstrated as follows:

Table I. Possible Combinations of Polarizer and Analyzer Resulting in the Identification of Relevant Scattering Matrix Elements for Spherical Particles

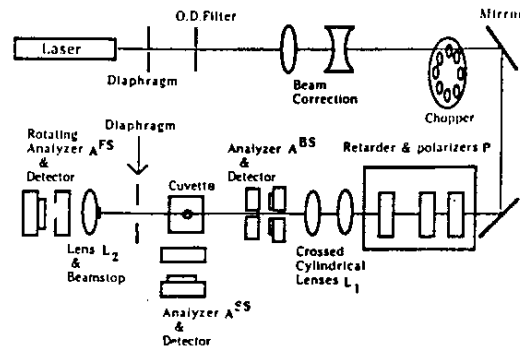| A \ P	U	$P_{\parallel}$	$P_{\perp}$	P_+	P_-	P_R	P_L
U	S_{11}	$\frac{1}{2}(S_{11}+S_{12})$	$\frac{1}{2}(S_{11}-S_{12})$	$\frac{1}{2}S_{11}$	$\frac{1}{2}S_{11}$	$\frac{1}{2}S_{11}$	$\frac{1}{2}S_{11}$
$A_{\parallel}$	$\frac{1}{2}(S_{11}+S_{12})$	$\frac{1}{2}(S_{11}+S_{12})$	0	$\frac{1}{4}(S_{11}+S_{12})$	$\frac{1}{4}(S_{11}+S_{12})$	$\frac{1}{4}(S_{11}+S_{12})$	$\frac{1}{4}(S_{11}+S_{12})$
$A_{\perp}$	$\frac{1}{2}(S_{11}-S_{12})$	0	$\frac{1}{2}(S_{11}-S_{12})$	$\frac{1}{4}(S_{11}-S_{12})$	$\frac{1}{4}(S_{11}-S_{12})$	$\frac{1}{4}(S_{11}-S_{12})$	$\frac{1}{4}(S_{11}-S_{12})$
A_+	$\frac{1}{2}S_{11}$	$\frac{1}{4}(S_{11}+S_{12})$	$\frac{1}{4}(S_{11}-S_{12})$	$\frac{1}{4}(S_{11}+S_{33})$	$\frac{1}{4}(S_{11}-S_{33})$	$\frac{1}{4}(S_{11}+S_{34})$	$\frac{1}{4}(S_{11}-S_{34})$
A_-	$\frac{1}{2}S_{11}$	$\frac{1}{4}(S_{11}+S_{12})$	$\frac{1}{4}(S_{11}-S_{12})$	$\frac{1}{4}(S_{11}-S_{33})$	$\frac{1}{4}(S_{11}+S_{33})$	$\frac{1}{4}(S_{11}-S_{34})$	$\frac{1}{4}(S_{11}+S_{34})$
A_R	$\frac{1}{2}S_{11}$	$\frac{1}{4}(S_{11}+S_{12})$	$\frac{1}{4}(S_{11}-S_{12})$	$\frac{1}{4}(S_{11}+S_{34})$	$\frac{1}{4}(S_{11}-S_{34})$	$\frac{1}{4}(S_{11}+S_{34})$	$\frac{1}{4}(S_{11}-S_{34})$
A_L	$\frac{1}{2}S_{11}$	$\frac{1}{4}(S_{11}+S_{12})$	$\frac{1}{4}(S_{11}-S_{12})$	$\frac{1}{4}(S_{11}-S_{34})$	$\frac{1}{4}(S_{11}+S_{34})$	$\frac{1}{4}(S_{11}-S_{34})$	$\frac{1}{4}(S_{11}+S_{34})$

Fig. 3. Outline of the optical configuration for polarization experiments in our flow through system.

$$S_{out} = \bar{A}_+ \bar{M} \bar{P}_{\parallel} \bar{S}_{in}, \qquad (8)$$

where

$$\bar{A}_+ = \frac{1}{2} \begin{bmatrix} 1 & 0 & 1 & 0 \\ 0 & 0 & 0 & 0 \\ 1 & 0 & 1 & 0 \\ 0 & 0 & 0 & 0 \end{bmatrix} \quad \text{and} \quad \bar{P}_{\parallel} = \frac{1}{2} \begin{bmatrix} 1 & 1 & 0 & 0 \\ 1 & 1 & 0 & 0 \\ 0 & 0 & 0 & 0 \\ 0 & 0 & 0 & 0 \end{bmatrix},$$

$\bar{M}$ is the scattering matrix defined by Eq. (4), and $\bar{S}_{in}$ is the Stokes vector of the incident light $[\bar{S}_i = (1,0,0,0)$ for unpolarized light]. Evaluating Eq. (8) results in a Stokes vector for the scattered light:

$$S_{out} = \frac{1}{4}(S_{11} + S_{12}, 0, S_{11} + S_{12}, 0)^T.$$

The observed detector signal is proportional to the first element of $\bar{S}_{out}$ [see Eq. (1)]. Accordingly, it can be shown that combination $\{P_{\perp}, A_+\}$ results in

$$S_{out} = \frac{1}{4}(S_{11} - S_{12}, 0, S_{11} - S_{12}, 0)^T.$$

As a consequence S_{11} and S_{12} can be derived individually from these measurements. Corresponding combinations of $\{P_x, A_y\}$ resulting in different elements of Eq. (4) are listed in Table I, where U denotes the absence of a polarizing filter (unpolarized light).

Since the scattering matrix [Eq. (4)] is highly symmetrical, many combinations of $\{P_x, A_y\}$ lead to the same result. This intrinsic characteristic of the scattering matrix for spheres can be exploited to verify the consistency of the experiment. It can be concluded that investigation of the bold-faced combinations in Table I is sufficient if particles of spherical symmetry are considered.

A. Experimental Configuration

Figure 3 illustrates the arrangement of the optical elements in our flow through equipment. Linear polarized monochromatic light from an argon-ion laser (Innova 70 Coherent) or from a He–Ne laser (10 mW Spectra Physics) provides the incident light. A construction of beam shaping optics consisting of a diaphragm, a neutral optical density filter, and a set of lenses modifies the incident beam to a suitable intensity and beam shape (argon laser beam diameter = 1.4 mm; He–Ne laser beam diameter = 1.9 mm). The laser beam passes a chopper and is directed by means of two mirrors onto the polarizing filter P. The latter

consists of two linear polarizers and a retarder (quarter lambda plate). Two crossed cylindrical lenses focus the incident beam on the flow channel (see also Fig. 2). The scattered light is measured by three detectors in the FS, SS, and BS directions.[4] Each detector is equipped with an appropriate analyzer A^i (i = FS,SS,BS). In addition a beam stop is inserted in the FS detector to remove the incident light from the scattered light. Lens L_2 is used to increase the numerical aperture of the FS detector ($1.0° < FS < 7.2°$; $78.2° < SS < 101.8°$; $160.6° < BS < 173.9°$).

A well-known error introduced by large numerical apertures is the so-called aperture depolarization. Nevertheless, it can be shown that in our optical system these types of artifact are negligible (see the Appendix).

Each time a particle passes the focused laser beam, a light pulse is measured by the detectors. This pulse is amplified and registered by a pulse height analyzer. In calibration measurements the light pulses are simulated by the chopper.

B. Calibration of the Equipment

The Stokes vector of the scattered light, measured with the optical arrangement discussed above, is described by

$$S_{out} = \bar{A}_y^i \bar{O}_2^i \bar{M} \bar{O}_1 \bar{P}_x S_{in}. \qquad (9)$$

where perturbation matrix $\bar{O}_1$ is the Mueller matrix describing the polarization characteristics of the optical elements between the polarizer ($\bar{P}_x$) and the scatterer ($\bar{M}$). Perturbation matrix $\bar{O}_2^i$ contains the polarizing characteristics of the equipment between the scatterer and the analyzer $\bar{A}_y^i$ (i = FS,SS,BS). In this section we describe a calibration method to correct for the errors introduced by these perturbations.

It is assumed that the complete Mueller matrix of the cuvette can be divided into four independent matrices related to the three principal directions (FS,SS,BS) (see Fig. 4).

The primary light beam, incident on the particles, is first modified by the Mueller matrix $\bar{C}_1$. In addition, the scattered light in the SS direction is modified by $\bar{C}_2$ (or $\bar{C}_4$), in the FS direction by $\bar{C}_3$, and in the BS direction by $\bar{C}_1^{-1}$. In the sequel we will incorporate the perturbation $\bar{L}_1$, $\bar{C}_{1,2,3}$, and $\bar{L}_2$ into the perturbation matrices $\bar{O}_1$ and $\bar{O}_2^i$ ($\bar{L}_1$ and $\bar{L}_2$ refer to the Mueller matrices of the crossed cylindrical lenses and the lens in the forward scattering direction, respectively):

$$\bar{O}_1 = \bar{C}_1 \bar{L}_1,$$
$$\bar{O}_2^{FS} = \bar{L}_2 \bar{C}_3, \quad \bar{O}_2^{SS} = \bar{C}_2, \quad \text{and} \quad \bar{O}_2^{BS} = \bar{C}_1^{-1}. \qquad (10)$$

Further reduction of Eqs. (9) and (10) can be obtained by investigation of the general structure of the Mueller matrices of the two lenses and the cuvette. It was verified experimentally that the polarization state of linear, perpendicular, or parallel polarized light, incident on any of these optical elements, was conserved. In accordance with this observation, the general Mueller matrix $\bar{Q}$ (4 × 4 terms) of the perturbating object reduces to
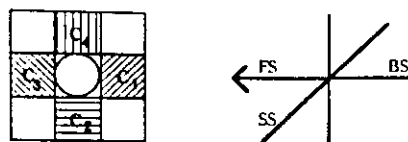
Fig. 4. Mueller matrices C_{1-4} describe the complete cuvette in the three principal directions.

$$\begin{bmatrix} q_{11} & q_{12} & q_{13} & q_{14} \\ q_{12} & q_{11} & q_{23} & q_{24} \\ 0 & 0 & q_{33} & q_{34} \\ 0 & 0 & q_{43} & q_{44} \end{bmatrix}. \qquad (11)$$

Equations (100)–(104) from Hovenier et al.[32] allow a further reduction of Eq. (11):

$$\begin{bmatrix} q_{11} & q_{12} & 0 & 0 \\ q_{12} & q_{11} & 0 & 0 \\ 0 & 0 & q_{33} & q_{34} \\ 0 & 0 & -q_{34} & q_{33} \end{bmatrix}. \qquad (12)$$

This matrix is in exact resemblance with the scattering matrix for a sphere $\bar{M}$ [Eq. (4)] and in addition commutates with $\bar{M}$: ($\bar{M}\bar{Q} = \bar{Q}\bar{M}$).

It is assumed that $\bar{C}_1 = \bar{C}_2 = \bar{C}_3 = \bar{C}_4 = \bar{C}$ with symmetry properties corresponding to the matrix Eq. (12) (it was verified experimentally that $\bar{C}_1 \times \bar{C}_3 = \bar{C}_2 \times \bar{C}_4$). As a consequence Eq. (9) can be evaluated using Eq. (10) and the commutation of the various matrices:

$$S_{out}^{FS} = \bar{A}_y^{FS} \bar{M} \bar{L}_2 \bar{C} \bar{C} \bar{L}_1 \bar{P}_x S_{in}, \qquad (13a)$$

$$S_{out}^{SS} = \bar{A}_y^{SS} \bar{M} \bar{C} \bar{C} \bar{L}_1 \bar{P}_x S_{in}, \qquad (13b)$$

$$S_{out}^{BS} = \bar{A}_y^{BS} \bar{M} \bar{L}_1 \bar{P}_x S_{in}. \qquad (13c)$$

These equations imply that the combined error introduced by the optics can be described by a single perturbation matrix $\bar{O}^i$. Therefore, we can investigate the complete error by simply measuring the matrix $\bar{O}^i$. The symmetry of $\bar{O}^i$ corresponds to the scattering matrix $\bar{M}$ [Eq. (4)]; hence we can determine the elements of the perturbating matrices ($\bar{O}^{FS}$, $\bar{O}^{SS}$, $\bar{O}^{BS}$) by measuring the bold-faced combinations shown in Table I. For forward scattering ($\bar{O}_{FS} = \bar{L}_2 \bar{C} \bar{C} \bar{L}_1$), we obtain

$$\bar{O}^{FS} = \begin{bmatrix} 1.00 & 0.09 & 0.00 & 0.00 \\ 0.09 & 1.00 & 0.00 & 0.00 \\ 0.00 & 0.00 & 0.96 & 0.29 \\ 0.00 & 0.00 & -0.29 & 0.96 \end{bmatrix}. \qquad (14a)$$

Measurement of $\bar{O}^{SS}(= \bar{C} \bar{C} \bar{L}_1)$ resulted in

$$\bar{O}^{SS} = \begin{bmatrix} 1.00 & 0.02 & 0.00 & 0.00 \\ 0.02 & 1.00 & 0.00 & 0.00 \\ 0.00 & 0.00 & 0.97 & 0.26 \\ 0.00 & 0.00 & -0.26 & 0.97 \end{bmatrix}. \qquad (14b)$$

whereas $\bar{O}^{BS}(= \bar{L}_1)$ resulted in

$$\bar{O}^{BS} = \begin{bmatrix} 1.00 & 0.00 & 0.00 & 0.00 \\ 0.00 & 1.00 & 0.00 & 0.00 \\ 0.00 & 0.00 & 0.99 & 0.16 \\ 0.00 & 0.00 & -0.16 & 0.99 \end{bmatrix}. \qquad (14c)$$

From these measurements it can be concluded that the perturbation matrices $\tilde{O}^i$ vary significantly from the unit matrix (where no perturbation is observed). Especially the $\tilde{O}_{34}$ terms introduce strong mixing between the S_{33} and S_{34} elements. As a consequence errors in the measurement of S_{33} and S_{34} will occur. Obviously a correction must be applied to correct for these perturbations. We therefore introduce the following procedure to correct the incident light in such a way that the perturbations are unambiguously eliminated. From Eqs. (13a)-(13c) it follows that

$$S^i_{out} = \bar{A}^i_y \tilde{M} \tilde{O}^i \tilde{P}_x S_{in}. \tag{15}$$

Due to the commutativity of the involved Mueller matrices, we can interpret Eq. (15) as though the complete optics is situated in front of the illuminated particle. Therefore compensation of the perturbations introduced by the complete optics is straightforward: adjust the polarization filter P (see Fig. 3) in such a way that the desired polarization is obtained, after the light has passed the relevant optical elements (without particles in the flow system). Evidently, the errors introduced by the optics can be corrected for without detailed numerical knowledge of the perturbation matrices.

IV. Results

In this section measurements and theoretical calculations of scattering matrix elements of monodisperse polystyrene spheres in a flow through system are presented.

Since the gross cell size of human blood cells varies from ~3 to ~15-μm (diameter) and the range of the

incident wavelength (λ) is 450 nm $\leq \lambda \leq$ 650 nm, the possible range of the size parameter α ($2\pi r/\lambda$) is 15 $\leq \alpha \leq$ 100. Four different values of α in this range were studied (see Table II). The tabulated size parameter α was calculated in accordance with the following equation[33]:

$$\alpha = \frac{2\pi r}{\lambda_{med}},$$

where $\lambda_{med} = \lambda_{vac}/\eta_{med}$ and

$$\eta_{med} = 1.3236 + \frac{3.35 \times 10^{-3}}{\lambda^2_{vac}} - \frac{3.45 \times 10^{-5}}{\lambda^4_{vac}}.$$

Here λ_{vac} (λ in μm) is the wavelength in vacuum, λ_{med} is the wavelength in the medium (water), and η_{med} is the refractive index of the medium.

For each α in Table II the bold-faced combinations $\{P_x, A_y\}$ from Table I were measured. The results are shown in Table III. The intensities correspond to the observed channel numbers of a pulse height analyzer. The values in parentheses denote the measured standard deviation. The data from this table indicate that the combined error introduced by the complete experimental equipment (Fig. 3) $\approx$5%.

From Table III the normalized elements $S_{12}/S_{11}, S_{33}/S_{11}, S_{34}/S_{11}$ are calculated for each α and each direction (FS,SS,BS). The results are shown in Table IV.

The standard error in parentheses (Table IV) is calculated in accordance with[34]

Table II. Size Parameters α of the Polystyrene Spheres Investigated in this Study; the Value of the Wavelength Is Relative to Vacuum; the 476- and 488-nm Wavelengths were Obtained from an Argon-Ion Laser, Whereas the 632.8-nm Line was Obtained from a He–Ne Laser

λ_{vac} (nm)	476 nm	488 nm	632.8 nm
r (μm)*			
2.46 ± 0.05	43.36	—	32.47
4.94 ± 0.04	—	85.04	65.34

* Data Scientific Polystyrene microspheres 1135D. San Antonio, Palo Alto, CA 94303

Table IV. Scattering Matrix Elements for Various Size Parameters and Directions Measured in a Flow Through System; the Standard Errors are In Parentheses

	α_1 (32.47)			α_2 (43.36)			α_3 (65.34)			α_4 (85.04)		
	FS	SS	BS	FS	SS	BS	FS	SS	BS	FS	SS	BS
S_{12}/S_{11}	0.00 (0.00)	-0.10 (0.05)	0.01 (0.01)	0.20 (0.10)	-0.62 (0.05)	-0.04 (0.01)	0.00 (0.00)	-0.35 (0.05)	0.01 (0.05)	0.00 (0.00)	-0.54 (0.05)	0.00 (0.00)
S_{33}/S_{11}	1.00 (0.05)	0.34 (0.05)	-0.79 (0.05)	1.00 (0.05)	0.38 (0.05)	-0.61 (0.05)	1.00 (0.10)	0.39 (0.05)	-0.71 (0.10)	1.00 (0.05)	0.15 (0.01)	0.68 (0.05)
S_{34}/S_{11}	0.00 (0.00)	-0.40 (0.10)	-0.16 (0.05)	0.00 (0.00)	0.12 (0.05)	-0.25 (0.05)	0.00 (0.05)	-0.11 (0.05)	-0.16 (0.10)	0.00 (0.00)	-0.15 (0.05)	-0.33 (0.05)

Table III. Measured Intensities in Three Directions for Four Size Parameters; the Values Correspond to a Mean Channel Number Obtained by Means of a Pulse Height Analyzer. The Number of Independent Observations Per Size Parameter Per Direction is 9; the Standard Deviation is Tabulated in Parentheses

		α_1 = 32.47			α_2 = 43.36			α_3 = 65.34			α_4 = 85.04		
$\{P_x, A_y\}$	Measured terms	FS	SS	BS	FS	SS	BS	FS	SS	BS	FS	SS	BS
|↑, →|	$1/4(S_{11} + S_{12})$	107 (4)	86 (10)	64 (2)	50 (4)	28 (4)	61 (2)	56 (3)	204 (5)	47 (3)	28 (1)	115 (3)	104 (1)
|⊥, →|	$1/4(S_{11} - S_{12})$	108 (5)	105 (4)	58 (1)	32 (4)	120 (6)	56 (2)	58 (3)	99 (4)	46 (3)	30 (1)	34 (2)	89 (1)
|→, →|	$1/4(S_{11} + S_{33})$	178 (8)	128 (5)	16 (3)	77 (3)	84 (2)	23 (3)	111 (9)	165 (7)	13 (1)	60 (1)	92 (1)	33 (2)
|↖, →|	$1/4(S_{11} - S_{33})$	0 (-)	63 (3)	140 (5)	0 (-)	38 (3)	94 (4)	0 (-)	74 (2)	78 (8)	0 (-)	68 (2)	174 (7)
|R, →|	$1/4(S_{11} + S_{34})$	112 (8)	56 (7)	80 (7)	40 (1)	68 (3)	44 (2)	54 (2)	106 (2)	64 (11)	51 (2)	67 (4)	62 (2)
|L, →|	$1/4(S_{11} - S_{34})$	113 (4)	131 (10)	111 (10)	38 (1)	53 (3)	72 (2)	58 (2)	132 (4)	88 (7)	51 (2)	91 (4)	123 (4)

$$S_{ret} = \left[\left[\frac{1}{\bar{x}_{nom}}\right]^2 + \left[\frac{1}{\bar{x}_{denom}}\right]^2\right]^{1/2} \cdot S \cdot R,$$

where

$$R = \frac{\bar{x}_1 - \bar{x}_2}{\bar{x}_1 + \bar{x}_2} = \frac{\bar{x}_{nom} \pm S}{\bar{x}_{denom} \pm S}, \quad \text{and} \quad S = [S_1^2 + S_2^2]^{1/2}.$$

$\bar{X}_1, \bar{X}_2$ refer to the measured terms listed in Table III, and R denotes the normalized scattering matrix elements from Table IV.

To investigate the reliability of the measured elements, theoretical calculations of the scattering matrix elements by means of a modified Mie program that incorporates the localization principle were performed. Calculation of the scattering elements, however, requires knowledge of the actual beam waist radius in the focal plane. We therefore investigated, by means of two alternative methods, the real beam waist. First the beam correcting optics were reverted to estimate the beam spot incident on the crossed cylindrical lenses (Fig. 3) (several combinations of the convergent and divergent lenses were studied). Subsequently, the beam spot in the cuvette, after focusing by the crossed cylindrical lenses ($f_1 = 7.5 \times 10^{-2}$ m, $f_2 = 1.5 \times 10^{-2}$ m) can be derived from Eq. (16). The beam waist radius is proportional to the incident wavelength (λ_{vac})[35]:

$$\omega_0 = \frac{4}{\pi} \frac{\lambda_{vac}}{\omega} f_2, \tag{16}$$

where ω is the beam waist of the incident light and f_2 is the focal length of the second cylindrical lens ($f_2 \ll f_1$) (see Fig. 3). Another method is to measure the pulse width of the scattered light of small particles ($d_{part} \ll d_{beam}$) passing the focused laser beam. Given the particle flow rate, the beam waist radius can be calculated directly. This resulted, for both the He–Ne laser and the Ar-ion laser, in

$$\bar{\omega}_{meas} = 3.3 \pm 1.2 \ \mu m.$$

To allow comparison of the calculations for various wavelengths, the numerical values of ω were normalized to $\lambda = 632.8$ nm [Eq. (16)]. The refractive index for polystyrene spheres was calculated from[33]

$$\eta_{poly} = 1.5711 + \frac{4.82 \times 10^{-3}}{\lambda_{vac}^2} + \frac{6.78 \times 10^{-4}}{\lambda_{vac}^4}.$$

To the best of our knowledge, the influence of small changes in the beam waist on the scattering matrix elements has not been reported in the literature. We therefore studied numerically the relation between the beam waist radius and the scattering matrix elements. The elements were calculated for each α and each direction as a function of the beam waist radius (1.0 μm $\leq \omega_0 \leq 10.0 \ \mu$m, relative to $\lambda_{vac} = 632.8$ nm). A typical example of these calculations, in the BS direction, for $\alpha = 43.36$ is shown in Fig. 5.

It is observed from Fig. 5 that, for the beam waist radii of interest, small changes in the beam waist may reflect relatively large changes in the calculated scattering elements (see, for example, the S_{33}/S_{11} dependence on ω). On the other hand, small deviations in
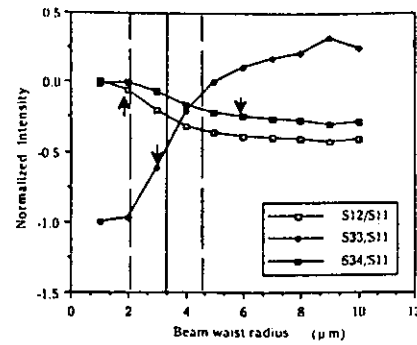

Fig. 5. Numerical simulation of the influence of the normalized scattering elements in the BS direction for $a = 43.36$. The arrows indicate the measured values obtained with our flow through equipment (see also Table IV). The solid vertical line indicates the mean measured beam waist whereas the broken vertical lines are determined by the corresponding standard deviation.
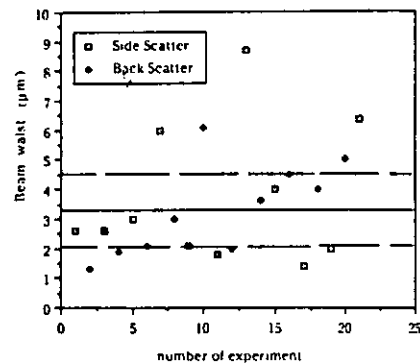

Fig. 6. Beam waist corresponding to the experimentally derived scattering matrix elements. The solid line indicates the measured mean beam waist value. The broken lines indicate the related standard deviation.

the measured values of the scattering matrix elements may introduce a significant uncertainty in the beam waist radius that should be applied in the numerical calculations (see, for example, the S_{12}/S_{11} and S_{34}/S_{11} dependence on ω). These phenomena are present for all α terms and all scattering directions studied (data not shown). It is our opinion therefore that reliable interpretation of the measured scattering matrix elements (Table IV) can be obtained through calculations similar to those presented in Fig. 5. Therefore for each direction studied we calculated the beam waist corresponding to the measured scattering matrix elements. The results for the SS and BS directions for $\alpha_{1..4}$ are summarized in Fig. 6. Statistical analyses of the beam waists from Fig. 6 resulted in

$$\bar{\omega}_0 = 3.5 \pm 2.0 \ \mu m.$$

V. Discussion

A. Experimental Setup and Measurement of the Scattering Matrix Elements

The specific experiments reported in this paper have concentrated on the measurement of the scattering matrix of well-defined spheres resembling the scatter-

ing matrix of biological particles in flow. One of the major problems arising in this type of experiment is related to the extreme short sampling time per cell (≈ 10 μs). In addition, there is a severe deficiency in Our knowledge concerning which scattering matrix elements of biological particles are of fundamental interest. Research with respect to this problem was reported by Bickel et al.[15,36] They showed from experimental data that especially the S_{34} element is a unique indicator of biological scatterers in suspension. Nevertheless, other elements, not studied in detail, may also contribute to the differentiation of biological particles. It is intelligible however, that measurement of all the scattering elements is nearly impossible and perhaps not necessary when flow through experiments are involved.

Experiments in a flow through system (i.e., a flow cytometer) are mainly concerned with finite (sub)populations of cells.[3] Therefore, characterization of the complete (sub)population is of main interest. Apparently, we are forced to investigate the scattering matrix of an ensemble of cells, instead of the scattering matrix of a single cell. Fortunately, symmetry conditions, especially valid for an ensemble of cells measured in a flow system, reduce the number of independent matrix elements to six [see Sec. II and Eq. (3)]. Three characteristics of a flow cytometer are exceedingly important here:

(1) Cells are measured one by one; this results in single scattering and allows simple (incoherent) addition of the scattering matrices of each cell studied.

(2) Cells are randomly oriented on passing the laser beam; therefore ensemble averaging can be applied.

(3) The average signal of the complete ensemble is studied; as a consequence variations introduced by imperfections of the hydrodynamically focused flow, misalignments in the optics, and biological spread are automatically compensated for.

These three characteristics, implicit in a flow through experiment, contribute positively to the light scattering (de)polarization measurements of biological cells. On the other hand, however, the complete optical equipment demands some experimental and theoretical adaptations:

(1) The sharply focused laser beam constrains the theoretical description of the interaction of a particle with the laser beam. Interpretation of the obtained data must therefore include a more sophisticated scattering theory. In the previous theoretical section we implemented the localization principle into a Mie program to account for this specific beam shape effect. (It should be noted that an axisymetric beam shape was implicit in our calculations, whereas the actual beam does contain an elliptical section.)

(2) The special purpose optics introduces some experimental errors. It was shown that these perturbations can be deleted by adequate adjustment of the incident beam.

To investigate the possibility of application of a flow through system to measure the six relevant scattering matrix elements of biological cells

($S_{11},S_{12},S_{22},S_{33},S_{34},S_{44}$), a test system with exactly known scattering characteristics must be studied. It is obvious that the measurement of spheres in the size regime of biological cells ($10 \leq \alpha \leq 100$) allows us to test the parameters of the adapted theory (i.e., beam waist) and the experimental setup. However, it is implicit in this test system of spheres that no differentiation between S_{22} and S_{11} or S_{33} and S_{44} can be obtained [see Eq. (4)]. Therefore, the consistency of $S_{22} = S_{11}$ was checked by additional measurement of the combinations $\{P_\parallel,A_\parallel\}$, $\{P_-,A_\parallel\}$, and $\{P_\perp,A_\parallel\}$, resulting in $1/4(S_{11} + 2S_{12} + S_{22})$, $1/4(S_{11} + S_{12})$, and $1/4(S_{11} - S_{22})$, respectively. From these measurements S_{22} and S_{11} could be derived. No differences in S_{11} and S_{22} were detected. Measurement of the S_{44} term was omitted since it requires a retarder analyzer. This would introduce inevitable complications especially for the measurement of the BS signal. The consistency of $S_{33} = S_{44}$ in the FS and SS directions was verified.

To explore the extent to which the four remaining scattering elements can be measured, a number of independent experiments were performed (see Tables II, III, and IV). From Table III it can be seen that the experiments are reproducible to within 5%. Furthermore it was observed that $S_{12} = S_{21}$ and $S_{34} = -S_{43}$ (data not shown). The data in Table IV indicate, after detailed statistical analysis, that the scattering matrix elements S_{ij} can be obtained with an accuracy of approximately $S_{ij} \pm 0.05$.

Still, however, no information was present about the correlation between the experimentally derived elements and the corresponding theoretical values. In a first approach to fit these data to theoretical values, no significant correlation could be discerned. We therefore investigated the influence of the sharply focused laser beam on the calculated scattering profile by means of numerical simulations. An example of this simulation was depicted in Fig. 5. Insertion of the measured values showed that the corresponding beam waist radii are grouped around 3.5 μm (Fig. 6). As was shown in the previous section, the estimated beam waist radius and the numerically calculated beam waist radius are approximately equal. We therefore conclude that after implementation of the beam waist radius the measured terms of the scattering matrix correspond quantitatively with the calculated values.

B. Light Scattering by Biological Particles

In the remaining part of this section we discuss in more detail the theoretical regime to which the light scattering of human blood cells is confined. A concise overview of available theories is illustrated in Fig. 7.

In a previous paper we introduced the concentric sphere structure as a possible model for human peripheral lymphocytes.[12,13] Here it is assumed that the two compartments of a concentric sphere mimic both the cytoplasm and the nucleus of the blood cells. It was confirmed recently, by means of osmotic shock experiments, that this model is well suited to describe at least the forward light scattering of human blood lymphocytes measured in a flow through system.[14] However,

backscattering directions the following phenomena occur: For decreasing values of m both S_{12}/S_{11} and S_{33}/S_{11} reach a constant value at $m \approx 1.010$, whereas S_{34}/S_{11} still varies significantly from its end value (data not shown). This anomalous behavior of S_{34}/S_{11} vs S_{33}/S_{11} can be explained by means of the following considerations: for spherical particles the amplitude functions S_3 and S_4 are identical to zero. This implies that $S_{33} = \mathrm{Re}(S_1 S_2^*)$ and $S_{34} = \mathrm{Im}(S_2 S_1^*)$.[19] After substitution of S_1 by $A_1 \exp(i\phi_1)$ and S_2 by $A_2 \exp(i\phi_2)$ this set of equations becomes $S_{33} = A_1 A_2 \cos\delta$, $S_{34} = -A_1 A_2 \sin\delta$, and $S_{11} = |A_1|^2 + |A_2|^2$, where $\delta = (\phi_1 - \phi_2)$. First-order expansion of these goniometric functions results in

$$S_{33}/S_{11} \sim 1 - \tfrac{1}{2}\delta^2 \quad \text{and} \quad S_{34}/S_{11} \sim -\delta.$$

Apparently, for small a phase shift δ (the RDG limit), S_{33} will converge to 1, whereas S_{34} still deviates significantly from zero. In conclusion: although the light scattering characteristics of human blood cells are dictated by the RDG regime (to a first approximation), some (de)polarization information, at least in the S_{34} terms, must be present. We therefore stipulate the necessity to measure in flow through systems:

S_{12}/S_{11} (cross polarization defined by Zerull et al.[38]);

S_{22}/S_{11} or S_{33}/S_{44} (information on spherical symmetry of the particles)[19]; and

S_{34}/S_{11} (information on subtle morphological differences).[15]

In addition mRDG[12-14] and RDG[19,20] approximations can be applied to predict the behavior of the S_{11} element of (low symmetry) biological particles.

VI. Conclusions

We have demonstrated that quantitative measurement of the scattering matrix elements of biological particles can be performed in flow through equipment. It has been shown that theoretical simulation of this type of experiment requires implementation of the beam shape into Mie scattering functions a_n, b_n. In addition large cone integration must be applied to account for the relatively large detector surfaces.

Furthermore a model is proposed to describe the scattering matrix of biological particles in the RDG limit in flow. It was illustrated that (de)polarization must occur in biological particles. In the near future we shall concentrate on the discrimination and subsequent separation of human blood cells by means of this (de)polarization information. Pilot experiments, carried out with our flow through equipment,[4] confirmed the suggested behavior that the S_{34} element, in contrast to the S_{33} element, derived from human lymphocytes deviates significantly from the values implicit in the RDG approximation, thus indicating the validity of the proposed model.

Cell Model	Theory	Scattering matrix	Remarks
Homogeneous Sphere	Mie theory [19,20]	X	Exact: Size NR, m NR
	Generalized Lorenz Mie theory [16,28]	X	Exact: Size NR, m NR & Implementation of beam profile
	RDG [19,20]	B	Approximation: $\rho \ll 1$; $|m-1| \ll 1$
Concentric spheres	Mie-theory [19]	X	Exact: Size NR, m NR
	mRDG [12,13]	B	Applicable to human blood lymphocytes [12,13,14] Approximation: $\rho \ll 1$; $|m-1| \ll 1$
Arbitrary shape and composition	mRDG [12,13]	B	Approximation: $\rho \ll 1$; $|m-1| \ll 1$
	Symmetry considerations (This paper)	C	Ensemble averaging no analytical expressions

$$\bar{A} = \begin{bmatrix} S_{11} & S_{12} & 0 & 0 \\ S_{12} & S_{11} & 0 & 0 \\ 0 & 0 & S_{33} & S_{34} \\ 0 & 0 & -S_{34} & S_{33} \end{bmatrix} \quad \bar{B} = \begin{bmatrix} S_{11} & S_{12} & 0 & 0 \\ S_{12} & S_{11} & 0 & 0 \\ 0 & 0 & S_{33} & 0 \\ 0 & 0 & 0 & S_{33} \end{bmatrix} \quad \bar{C} = \begin{bmatrix} S_{11} & S_{12} & 0 & 0 \\ S_{12} & S_{22} & 0 & 0 \\ 0 & 0 & S_{33} & S_{34} \\ 0 & 0 & -S_{34} & S_{44} \end{bmatrix}$$

Fig. 7. Light scattering theories applicable to various cell models; NR means not restricted.

since the relative refractive index of human blood cells is close to unity, no (de)polarization information should be present. This is a consequence of the Rayleigh-Debye-Gans (RDG) approximation that is applied to particles that reveal this so-called index matching.[12,13,37] Application of the RDG approximation will result in a scattering matrix of type B (Fig. 7) that contains no particle dependent polarization information, since the phase shift ρ equals approximately zero ($\rho = 2\alpha|m - 1| \ll 1$).[20] Hence, the components of the matrix $\bar{B}$ can be described by (θ = scattering angle):

$$\bar{B} = \frac{1}{2} \begin{bmatrix} \cos^2\theta + 1 & -\sin^2\theta & 0 & 0 \\ -\sin^2\theta & \cos^2\theta + 1 & 0 & 0 \\ 0 & 0 & 2\cos\theta & 0 \\ 0 & 0 & 0 & 2\cos\theta \end{bmatrix}.$$

This notion is contradicted by various experiments demonstrating that particle dependent (de)depolarization is present in human blood cells.[15,17,36] Therefore, we examined theoretically the limits to which the RDG approximation can be applied for the three principal directions [Eq. (7)]. Numerical calculations with a Mie scattering program were performed for the region $1.00010 \le m \le 1.10000$, with size parameter $\alpha = 34.75$. The relative refractive index m refers to the optical density of a sphere. It was concluded from these data that especially in the side scattering and

Appendix

A possible error in the polarization measurements is introduced by the finite detector aperture. Light obtained from various regions of the solid detector angle will have different degrees of polarization due to the definition of the scattering plane. This so-called aperture depolarization is discussed in this Appendix for the geometry of the applied optical system.

Assume that the incident light, traveling in the positive z-direction, is linearly polarized in the x-direction and hits a sphere located at the origin (see Fig. 1). In the y-z plane (the scattering plane), the scattered light has the same perpendicular polarization as the incident light. However, an arbitrary point of the detector surface, not in the y-z plane, will define a new scattering plane. Thus, the incident light is no longer perfectly perpendicularly polarized with respect to this scattering plane but will have a small parallel component. As a consequence the scattered light also contains a small parallel component. This phenomenon is known as aperture depolarization.[39,17] In the sequel we shall derive a set of equations that allows calculation of the contribution of the aperture depolarization in our equipment.

The perpendicular and parallel components E_r^i and E_l^i of the incident electric field with respect to the new scattering plane are

$$E_l^i = \cos\phi \, E_x,$$
$$E_r^i = \sin\phi \, E_x. \qquad (A1)$$

The scattered fields are given by[20]

$$E_l^s = CS_2(\theta)E_l^i,$$
$$E_r^s = CS_1(\theta)E_r^i, \qquad (A2)$$

where C is a constant and $S_1(\theta), S_2(\theta)$ are the complex amplitude scattering functions. In polar coordinates (R,θ,ϕ) the scattered field components are

$$E_R^s = 0,$$
$$E_\theta^s = E_l^s, \qquad (A3)$$
$$E_\phi^s = -E_r^s.$$

Transformation of E_θ^s and E_ϕ^s to Cartesian coordinates (x,y,z) and application of Eqs. (A1) and (A2) result in

$$E_x^s(\theta,\phi) = CE_x[S_1(\theta)\sin^2\phi + S_2(\theta)\cos^2\phi\,\cos\theta],$$

$$E_y^s(\theta,\phi) = CE_x[-S_1(\theta)\sin\phi\,\cos\phi + S_2(\theta)\sin\phi\,\cos\phi\,\cos\theta], \quad (A4)$$

$$E_z^s(\theta,\phi) = CE_x[S_2(\theta)\cos\phi\,\sin\theta].$$

Apart from the last equality, Eq. (A4) is essentially the same as the equations used in Ref. 40. However, it can be shown that in the expressions used by Pal and Carswell, the scattering functions $S_{1,2}(\theta)$ are replaced by the square root of the phase functions $P_{1,2}(\theta)$.[20,40] Therefore, the phase information present in $S_{1,2}(\theta)$ is lost in their equations.

Assume that $\Delta\theta$, $\Delta\phi$ are $\ll 1$. This results in a detector surface that can be approximated by a small portion of a sphere with radius r. Then the expressions for the intensities of the components of the scattered field parallel and perpendicular to the polarization direction of the incident field $(I_\parallel, I_\perp)$ are:

In the forward scattering direction:

$$I_\parallel = r^2 \int_0^{2\pi} \int_0^{\Delta\theta} |E_x^s(\theta,\phi)|^2 \sin\theta d\theta d\phi,$$

$$(A5)$$

$$I_\perp = r^2 \int_0^{2\pi} \int_0^{\Delta\theta} |E_y^s(\theta,\phi)|^2 \sin\theta d\theta d\phi.$$

In the side scattering direction:

$$I_\parallel = r^2 \int_{\frac{\pi}{2}-\Delta\phi}^{\frac{\pi}{2}+\Delta\phi} \int_{\frac{\pi}{2}-\Delta\theta}^{\frac{\pi}{2}+\Delta\theta} |E_x^s(\theta,\phi)|^2 \sin\theta d\theta d\phi,$$

$$(A6)$$

$$I_\perp = r^2 \int_{\frac{\pi}{2}-\Delta\phi}^{\frac{\pi}{2}+\Delta\phi} \int_{\frac{\pi}{2}-\Delta\theta}^{\frac{\pi}{2}+\Delta\theta} |E_z^s(\theta,\phi)|^2 \sin\theta d\theta d\phi.$$

In the backscattering direction:

$$I_\parallel = r^2 \int_0^{2\pi} \int_{\pi-\Delta\theta}^{\pi} |E_x^s(\theta,\phi)|^2 \sin\theta d\theta d\phi,$$

$$(A7)$$

$$I_\perp = r^2 \int_0^{2\pi} \int_{\pi-\Delta\theta}^{\pi} |E_y^s(\theta,\phi)|^2 \sin\theta d\theta d\phi.$$

Assuming that for the forward scattering direction $S_{1,2}(\theta) \approx S_{1,2}(0)$ $(0 \le \theta \le \Delta\theta)$ and for the backscattering direction $S_{1,2}(\theta) \approx S_{1,2}(\pi)$ $(\pi - \Delta\theta \le \theta \le \pi)$ integration of Eqs. (A5) and (A7) results in (for both directions)

$$\frac{I_\perp}{I_\parallel} = \frac{(\Delta\theta)^4}{96}, \qquad (A8)$$

where $S_1(0) = S_2(0)$, $S_1(\pi) = -S_2(\pi)$ and are real functions.[20]

In the side scattering direction, integration of Eq. (A6) results in

$$\frac{I_\perp}{I_\parallel} = \frac{1}{3} \frac{\left|S_2\left(\frac{\pi}{2}\right)\right|^2}{\left|S_1\left(\frac{\pi}{2}\right)\right|^2} (\Delta\phi)^2, \qquad (A9)$$

where it is assumed that $S_{1,2}(\theta) \approx S_{1,2}(\pi/2)$ $(\pi/2 - \Delta\theta \le \theta \le \pi/2 + \Delta\theta)$.

Finally, we can calculate the aperture depolarization for our optical system. Inserting the detector apertures

forward scattering direction: $\Delta\theta = 0.13$ rad(7.2°),

side scattering direction: $\Delta\theta = 0.19$ rad(10.8°),

backscattering direction: $\Delta\theta = 0.34$ rad(19.4°)

into Eqs. (A8) and (A9) results in

forward scattering direction: $I_\perp/I_\parallel = 2.6 \times 10^{-6}$,

side scattering direction: $I_\perp/I_\parallel = 7.5 \times 10^{-3}$ (Ref. 41),

backscattering direction: $I_\perp/I_\parallel = 1.4 \times 10^{-4}$.

These errors, introduced by the finite aperture of the various detectors, are negligible.

The aperture depolarization for other polarizations of the incident beam can be calculated accordingly. From these calculations it was concluded that no significant aperture depolarization is present regardless

oɪ the polarization state oɪ the incident beam (data nɪ¢
shown).

References

1. M. R. Loken and A. M. Stall, "Flowcytometry as an Analytical and Preparative Tool in Immunology," J. Immunol. Methods 50, R85 (1982).
2. J. A. Steinkamp, "Flowcytometry," Rev. Sci. Instrum. 55, 1375 (1984).
3. M. A. van Dilla, P. N. Dean, O. D. Learum, and M. R. Melamed, Eds., Flowcytometry: Instrumentation and Data Analysis (Academic, London, 1985).
4. P. M. A. Sloot, M. J. Carels, P. Tensen, and C. G. Figdor, "Computer Assisted Centrifugal Elutriation. I: Detection System and Data Acquisition Equipment," Comp. Meth. Prog. Biomed. 24, 179 (1987).
5. G. C. Salzman et al., "Cell Classification by Laser Light Scattering: Identification and Separation of Unstained Leukocytes," Acta Cytol. 19, 374 (1975).
6. M. Bartholdi, G. C. Salzman, R. D. Hiebert, and M. Kerker, "Differential Light Scattering Photometer for Rapid Analysis of Single Particles in Flow," Appl. Opt. 19, 1573 (1980).
7. A. W. S. Richie, R. N. Gray, and H. S. Mickle, "Rightangle Light Scattering: A Necessary Parameter in Flow Cytofluorimetric Analysis of Human Peripheral Blood Mononuclear Cells," J. Immunol. Methods 64, 109 (1983).
8. J. M. Thompson et al., "The Optimal Application of Forward and Ninety Degree Light Scattering in Flowcytometry for the Gating of Mononuclear Cells," Cytometry 6, 401 (1985).
9. L. W. M. M. Terstappen et al., "Four-Parameter White Blood Cell Differential Counting Based on Light Scattering Measurements," Cytometry 9, 39 (1988).
10. G. R. Otten and M. R. Loken, "Two Color Light Scattering Identifies Physical Differences Between Lymphocytes Subpopulations," Cytometry 3, 182 (1982).
11. T. M. Jovin et al., "Automatic Sizing and Separation of Particles by Ratios of Light Scattering Intensities," J. Histochem. Cytochem. 24, 269 (1976).
12. P. M. A. Sloot and C. G. Figdor, "Elastic Light Scattering from Nucleated Blood Cells: Rapid Numerical Analysis," Appl. Opt. 25, 3559 (1986).
13. P. M. A. Sloot, "Elastic Light Scattering from Leucocytes in the Development of Computer Assisted Cell Separation," Ph.D. Thesis, Amsterdam, The Netherlands (1988).
14. P. M. A. Sloot, A. G. Hoekstra, and C. G. Figdor, "Osmotic Response of Lymphocytes Measured by Means of Forward Light Scattering: Theoretical Considerations," Cytometry 9, 636 (1988).
15. W. S. Bickel et al., "Application of Polarization Effects in Light Scattering: A New Biophysical Tool," Proc. Natl. Acad. Sci. U.S.A. 73, 486 (1976).
16. D. W. Schuerman, Ed., Light Scattering by Irregularly Shaped Particles (Plenum, New York, 1980).
17. B. G. de Grooth et al., "Light Scattering Polarization Measurements as a New Parameter in Flow Cytometry," Cytometry 8, 539 (1987).
18. G. Gouesbet, G. Gréhan, and B. Maheu, "Scattering of a Gaussian Beam by a Mie Scatter Center Using a Bromwich Formalism," J. Opt. 16, 83 (1985).
19. C. F. Bohren and D. R. Huffman, Absorption and Scattering of Light by Small Particles (Wiley, New York, 1983).
20. H. C. van de Hulst, Light Scattering by Small Particles (Dover, New York, 1981).

21. G. Gréhan, B. Maheu, and G. Gouesbet, "Scattering of a Laser Beam by Mie Scatter Centers: Numerical Results Using a Localized Approximation," Appl. Opt. 25, 3539 (1986).
22. B. Maheu, G. Gréhan, and G. Gouesbet, "Generalized Lorenz-Mie Theory: First Exact Values and Comparisons with the Localized Approximation," Appl. Opt. 26, 23 (1987).
23. J. T. Edsall, "Streaming Birefringence and Its Relation to Particle Size and Shape," Adv. Colloid Sci. 1, 270 (1942).
24. V. Kachel, "Basic Principles of Elastic Sizing of Cells and Their Realization in the New Instrument 'Metricell'," J. Histochem. Cytochem. 24, 211 (1976).
25. M. R. Loken, D. R. Parks, and L. Herzenberg, "Identification of Cell Asymmetry and Orientation by Light Scattering," J. Histochem. Cytochem. 25, 790 (1977).
26. V. Kachel, E. Kordwig, and E. Glossner, "Uniform Lateral Orientation, Caused by Flow Forces of Flat Particles in Flow-Through Systems," J. Histochem. Cytochem. 25, 774 (1977).
27. J. N. Lucas and D. Pinkel, "Orientation Measurement of Microsphere Doublets and Metaphase Chromosomes in Flow," Cytometry 7, 575 (1986).
28. G. Gouesbet, B. Maheu, and G. Gréhan, "Scattering of a Gaussian Beam by a Sphere Using a Bromwich Formulation: Case of an Arbitrary Location," in Optical Particle Sizing: Theory and Practice, G. Gouesbet and G. Gréhan, Eds. (Plenum, New York, 1988).
29. B. Maheu, G. Gouesbet, and G. Gréhan, "Laser Beam Scattering by Individual Spherical Particles: Numerical Results and Application to Optical Sizing," in Optical Particle Sizing: Theory and Practice, G. Gouesbet and G. Gréhan, Eds. (Plenum, New York, 1988).
30. W. S. Bickel and W. M. Bailey, "Stokes Vectors, Mueller Matrices, and Polarized Scattered Light," Am. J. Phys. 53, 468 (1985).
31. W. A. Shurcliff, Polarized Light: Production and Use (Harvard U.P., Cambridge MA, 1962).
32. J. W. Hovenier, H. C. van de Hulst, and C. V. M. van der Mee, "Conditions for the Elements of the Scattering Matrix," Astron. Astrophys. 157, 301 (1986).
33. E. Gulari et al., "Latex Particle Size Distributions from Multiwavelength Turbidity Spectra," Part. Charact. 4, 96 (1987).
34. J. R. Green and D. Margerison, Statistical Treatment of Experimental Data (Elsevier, Amsterdam, 1978).
35. J. F. Ready, Industrial Applications of Lasers (Academic, New York, 1978).
36. W. S. Bickel et al., "Biological Particles as Irregularly Shaped Scatterers," in Light Scattering by Irregularly Shaped Particles, D. W. Schuerman, Ed. (Plenum, New York, 1980), pp. 299–305.
37. W. S. Bickel, A. J. Watkins, and G. Videen, "The Light Scattering Mueller Matrix Elements for Rayleigh, Rayleigh-Gans, and Mie Spheres," Am. J. Phys. 55, 559 (1987).
38. R. H. Zerull, R. T. Killinger, and R. H. Gieze, "Optical Particle Sizing and Particle Characterization Based on Polarization Measurements," in Optical Particle Sizing: Theory and Practice, G. Gouesbet and G. Gréhan, Eds. (Plenum, New York, 1988).
39. T. Lindmo and H. B. Steen, "Flowcytometric Measurement of Fluorescence from Intracellular Fluorescence in Mammalian Cells," Biophys. J. 18, 173 (1977).
40. S. R. Pal and A. I. Carswell, "Polarization Anisotropy in Lidar Multiple Scattering from Atmospheric Clouds," Appl. Opt. 24, 3464 (1985).
41. From our Mie program it was calculated that $|S_2|^2/|S_1|^2 = 0.63$ for a polystyrene sphere in an aqueous medium.